

Constraining the Galactic Center Dark Cluster with ELT/MICADO Observations

Sebastiano D. von Fellenberg^{1,2,*}, Matúš Labaj³, and Sean M. Ressler¹

¹ Canadian Institute for Theoretical Astrophysics, University of Toronto, 60 St. George Street, Toronto, ON M5S 3H8, Canada

² Max Planck Institute for Radioastronomy, auf dem Hügel 69, Bonn, Germany

³ Department of Theoretical Physics and Astrophysics, Masaryk University, Kotlářská 2, 611 37 Brno, Czech Republic

Received September 30, 20XX

ABSTRACT

The Galactic Center hosts the densest known stellar environment in the Milky Way, dominated by the massive black hole Sgr A* and the surrounding nuclear star cluster. Theory predicts that this region should also contain a large population of stellar compact objects (SCOs)—black holes, neutron stars, and white dwarfs—forming a “dark cluster” whose distribution and properties remain observationally unconstrained. These unseen stellar remnants are central to questions of mass segregation, cluster dynamics, and the expected rate of extreme mass ratio inspirals (EMRIs) detectable by future gravitational-wave observatories including LISA. Current evidence for SCOs in the Galactic Center is indirect, relying on dynamical mass measurements, X-ray surveys, and a small number of transient sources. Direct detections remain elusive due to crowding, extinction, and the sensitivity limits of existing instruments. We explore how upcoming facilities, in particular the Extremely Large Telescope (ELT) with its first-light imager MICADO, can fundamentally transform this field. MICADO’s combination of deep photometry, high spatial resolution, and precise astrometry will enable systematic searches for SCO-star binaries via photometric variability and orbital astrometric signatures, as well as direct detection of isolated accreting black holes interacting with the gas-rich Galactic Center environment. We outline the observational pathways, technical challenges, and expected sensitivities, showing that ELT/MICADO observations can provide the first quantitative constraints on the dark cluster population. Establishing these constraints will be pivotal for understanding the dynamical evolution of the Galactic Center, the role of compact remnants in nuclear star clusters, and the astrophysical context of gravitational-wave sources in galactic nuclei.

Key words. Galactic Center – Black Holes – Nuclear Star Clusters – Gravitational Waves

1. Introduction

The Milky Way’s Galactic Center (GC) harbors the densest known star cluster, the nuclear star cluster (NSC). Since the early 1990s, modern telescopes have been able to track stellar motions in this region, which has revealed a concentration of a large, unseen mass of $\sim 4 \times 10^6 M_{\odot}$. This was ultimately proven to be a massive black hole (MBH) associated with the radio source Sgr A* (Genzel et al. 1997; Ghez et al. 2003). In the innermost region ($r < 1''$, e.g., Ghez et al. 2008; Gillessen et al. 2009), stars effectively behave as test particles, with their dynamics primarily governed by the potential of the MBH. Tracking their motion enables a precise determination of the black hole’s gravitational potential and allows one to test general relativistic effects on their orbits (GRAVITY Collaboration et al. 2018; Gravity Collaboration et al. 2020; Do et al. 2019). At larger distances ($r > 2''.5$, e.g., GRAVITY Collaboration et al. 2022), the mass of the NSC itself becomes relevant, and statistical tests can be used to infer the presence of an additional enclosed mass of $\approx 6 \times 10^6 M_{\odot}$ (e.g., Fritz et al. 2016).

Currently, only the most luminous stars are detectable because the light emitted from the Galactic Center (GC) is highly extinguished by dust along the line of sight (e.g., Fritz et al.

2011). Nevertheless, about 10^4 stars have been individually identified, and their presence implies that many stellar compact remnants (SCOs—stellar Compact Objects), such as black holes (BH), neutron stars (NS), or white dwarfs (WD), likely exist in the direct vicinity of the MBH (e.g., Miralda-Escudé & Gould 2000; Freitag et al. 2006; Schödel et al. 2020). Because these objects have so far largely eluded detection, their presence, distribution, and properties can only be estimated by theoretical models.

The question of how stars would settle around an MBH was first addressed by Peebles (1972), who argued that a steady state solution should exist in which there is a constant flux of stars through energy space, controlled by two-body interactions with a relaxation timescale, τ_{TB} . Building on this work, Bahcall & Wolf (1976) found that (equal-mass) stars settle into a power-law density profile, a so-called Bahcall—Wolf cusp:

$$n(r) \propto r^{-7/4}, \quad (1)$$

where $n(r)$ is the radial number density and r is the radial distance to the central mass. Bahcall & Wolf (1977) further extended this model to account for a multi-mass distribution and showed that the different scattering efficiencies lead to a phenomenon called mass segregation, where different masses settle into different power-law slopes. The heavier particles

* Humboldt Feodor Lynen Fellow

sink inward, while lighter particles get pushed to larger radii. This general result has been confirmed and quantified by subsequent analytical arguments and N-body simulations (e.g., Freitag et al. 2006; Alexander & Hopman 2009; Linial & Sari 2022; Zhang & Amaro Seoane 2024), which found that lighter stars should follow $n(r) \propto r^{-1.5}$, while the heavier components (such as stellar black holes) follow $n(r) \propto r^{-2}$.

Observationally, there is no direct confirmation of this otherwise clean theoretical prediction. The best stellar system at hand for direct tests, the GC, holds some surprises.

- The bright objects in the GC nuclear cluster do not comprise an old, relaxed system. Contrary to all predictions (e.g., Morris 1993), the GC is an efficient star-forming region (Krabbe et al. 1991; Paumard et al. 2006; Yelda et al. 2014). More than 200 recently formed Wolf-Rayet, O-, and B-type stars have been identified, with ages ~ 6 Myr and a top-heavy initial mass function (e.g., von Fellenberg et al. 2022; Jia et al. 2023). These stars are found in disk-like structures, likely reflecting gaseous structures from which they were formed and they are clearly dynamically unrelaxed.
- Further in, where the orbital periods are short enough for full orbital solutions to be determined (e.g., Gillessen et al. 2009; Boehle et al. 2016), the cluster of young stars also defies all theoretical expectations: it is in a relaxed and isotropic distribution, despite the fact that the stellar ages are much shorter than the local two-body relaxation time.
- Finally, the stars that come closest to the black hole (i.e., that have the smallest peri-center distance, R_p) are lighter than the stars at a larger radial distance (Burkert et al. 2024), again in stark contrast to the theoretical expectation of mass segregation.

These are long-standing riddles that have sparked interest in a broad community (e.g., Alexander 2017). One possibility is that the observed stellar population may well be a poor tracer for the governing bodies of the underlying dark cluster. Regardless, a key problem in modern astronomy is determining the rate at which SCOs merge with MBHs in galactic nuclei throughout the universe. Studying the gravitational waves emitted by these SCO-MBH mergers, called extreme-mass-ratio inspirals (EMRIs), are a key science goal of the Laser Interferometer Space Antenna (LISA; Amaro-Seoane et al. 2017). Because the distribution of SCOs is only (poorly) known theoretically, while unlikely to be zero, the number of EMRIs that LISA will observe is highly uncertain, with plausible estimates ranging from a few tens to several tens of thousands (Amaro-Seoane et al. 2007, 2012). A direct measurement of the SCO distribution in the GC would thus be the Rosetta stone for understanding the nuclear star cluster dynamics.

The Milky Way’s GC is a unique laboratory to study these phenomena, as it is the only galactic nucleus close enough to obtain direct quantitative constraints on the so far unseen objects orbiting around the MBH Sgr A*. This paper explores avenues toward detecting the dark cluster of SCOs in the GC, specifically those enabled by MICADO at the Extremely Large Telescope (ELT).

2. Current constraints on the Galactic Center dark cluster

2.1. Extended, dynamical mass

Observationally, the properties of the dark cluster are highly uncertain. The best constraints exist for the total mass contained

in the Galactic Center, derived from the measurement of position, proper motions, and (in some cases) radial velocities of thousands of luminous stars. These measurements indicate that the NSC can be modeled as a so-called “isotropic rotator”: stars move in random orientations but on average have the same sense of rotation as the Milky Way. Specifically, the total mass in the central 100 arcseconds of the galaxy is constrained to be $\sim 6 \times 10^6 M_\odot$ (e.g., Chatzopoulos et al. 2015; Fritz et al. 2016; Feldmeier-Krause et al. 2025).

At radial separations of a few arcseconds from Sgr A*, stellar orbital periods drop below 100 years, enabling precise determination of individual orbital elements. This is most strikingly exemplified by the star S2, the key tracer of Sgr A*’s mass (e.g., Ghez et al. 1998; Schödel et al. 2002; Gillessen et al. 2009, 2017; GRAVITY Collaboration et al. 2019). For stars with sufficiently short orbital periods, orbital solutions can simultaneously constrain both the mass of Sgr A* and the surrounding extended mass distribution. For instance, observations with GRAVITY have determined that the extended mass is $> 3000 M_\odot$ within the orbit of the star S2 ($r \approx 0''.23$), and $\sim 15000 M_\odot$ within $r \approx 3''$ of Sgr A* (GRAVITY Collaboration et al. 2022; Gravity Collaboration et al. 2024).

2.2. Stellar density profile

In addition to the dynamical information, the stellar density profile (i.e., the number of stars per area) can be measured and compared to the theoretically expected ones. For a long time, it was unclear whether the Galactic Center’s old giant star population indeed followed the expected relaxed Bahcall–Wolf cusp (e.g., Genzel et al. 2003; Schödel et al. 2007; Buchholz et al. 2009). More recent studies seem to indicate that, while brighter giant stars do not appear to follow the expected distribution, at least the fainter population does appear to be relaxed ($K_{\text{mag}} = 16 - 20$, e.g., Schödel et al. 2018; Habibi et al. 2019; Schödel et al. 2020).

2.3. Star formation history

The so-called K-band luminosity function (KLF) relates the number of stars to their luminosity and it encodes the formation history of the giant star population ($M_{\text{giant}} = 1 - 2 M_\odot$). Models of the KLF indicate that 80% of the Galactic Center giant stars formed along with the galaxy some ~ 13 Gyr ago. Nevertheless, subsequent star formation events occurred and contributed significantly to the present population, with major formation periods occurring $\approx 3 - 4$ Gyr and $0.2 - 0.5$ Gyr ago (e.g., Schödel et al. 2020), as evidenced by spectroscopic observations (Pfuhl et al. 2011). In addition, a small fraction of stars ($\sim 10^4 M_\odot$; Yelda et al. 2014) formed 6 Myr ago, i.e., the Young Star cluster mentioned previously. While the more recent work by Pfuhl et al. (2011) and Schödel et al. (2020) are in broad strokes consistent with each other and with previous work (e.g., Blum et al. 2003; Figer et al. 2004; Maness et al. 2007), Chen et al. (2023) measure a substantially different star formation history: they report a primary star formation event occurring just ~ 5 Gyr ago which formed 95% of the stellar mass. While the datasets of the different studies are comparable or complementary in depth and quality, Chen et al. (2023) argue that their more accurate metallicity modeling leads to the difference in the inferred cluster properties. The discussion of these differences is beyond the scope of this paper, and we adopt, in the following, values by Schödel et al. (2020) primarily because they lead to

more conservative estimates about the detectability of the dark cluster (i.e., the Chen et al. (2023) cluster model predicts compact objects that are easier to detect; see subsection 4.1 for more details).

2.4. Stellar binarity

Binaries play an important role in the Galactic Center: they enable the deposition of stars close to Sgr A* via the so-called Hills mechanism (Hills 1988; Generozov & Madigan 2020), strongly influence stellar dynamics (for a review, see Alexander 2017), and can provide luminous counterparts to otherwise undetectable SCOs. To date, only four binaries have been identified in the Galactic Center. All were discovered through dedicated variability studies, some of which were aided by spectroscopic follow-ups. To date, the most comprehensive studies were presented by Gautam et al. (2019, 2024), which were sensitive to binary periods ranging from ~ 1 to ~ 4000 days, and included 563 stars, of which roughly half were found to be intrinsically variable. A subset of 12 candidate binary stars was found (2% of the surveyed stars), three of which had variability on time scales of $P = 1 - 10$ days, five with $P = 1 - 80$ d, and four with $P > 80$ d. The binary system IRS 16SW has a photometric period of 9.6 days, with a minimum total mass of $100 M_{\odot}$ (Ott et al. 1999), and an equal mass ratio for the components (Martins et al. 2006, though note that these authors did not discuss the possibility of a star-SCO binary). The second known binary is IRS 16NE, which was discovered via radial velocity measurements, a long-period eclipsing binary with a period of ~ 200 days, a combined mass of $\sim 30 M_{\odot}$ and a mass ratio of 2 ± 0.5 . The third binary, E60, was again discovered via photometry and is a close eclipsing binary with an orbital period of roughly two days (Pfuhl et al. 2014). The fourth binary, S2-36, which shows a period of ~ 40 days, was discovered photometrically (Gautam et al. 2019) and confirmed by radial velocity measurements (Gautam et al. 2024). All of these binary systems are young stars, i.e., they were formed in the most recent star formation event ~ 6 Myr ago (e.g., Paumard et al. 2006; Yelda et al. 2014; von Fellenberg et al. 2022). In addition to those candidate systems, a few more candidate systems have been proposed, but have so far not been robustly confirmed: IRS29N shows features associated with a wind colliding binary (Rafelski et al. 2007); based on H-R diagram modeling Geballe et al. (2006) suggest IRS8 might be a binary; and IRS7E shows a large variability in radial velocity potentially consistent with a binary (Paumard et al. 2006). Most recently, Peißker et al. (2024) reported a binary system in a Galactic Center G-object.

2.5. Direct evidence for Galactic Center compact objects

So far, three bona fide direct measurements of SCOs in the Galactic Center have been reported. The first, XJ174540.0–290031, is a radio/X-ray transient that peaked at radio frequencies in 2004 (Bower et al. 2005; Porquet et al. 2005), located $2.9''$ from Sgr A*. Although its X-ray emission faded, it remains a compact radio source (Zhao et al. 2022), likely a quiescent low mass X-ray binary (qLMXB) or a free-floating SBH that underwent a strong accretion event. Notably, it comoves with the northern arm of the mini-spiral, potentially tapping into an additional gas reservoir (Bower et al. 2005). The second source, Sgr J1745–2900, is a magnetar located $\sim 2.4''$ from Sgr A*, first detected in X-rays (Eatough et al. 2013; Kennea et al. 2013) and later in radio (Bower et al. 2014). Its

proper motion aligns with the GC clockwise disk of young stars (Bower et al. 2015), suggesting it originated from the most recent star formation episode ~ 6 Myr ago. The third source, MAXI J1744–294, was discovered in early 2025 as an X-ray transient (e.g., Kudo et al. 2025) and subsequently in radio (e.g., Michail et al. 2025). Follow-up observations identify it as an LMXB (Mandel et al. 2025), and this conclusion has been consistently confirmed across multiple telescopes and groups (e.g., Marra et al. 2025; Chatterjee et al. 2025).

Beyond these three bona fide SCOs, several candidate sources have been reported. Zhao et al. (2022) conducted a deep JVLA survey of the central few arcseconds and identified dozens of compact radio sources. While some were linked to stellar winds based on their SED, a significant fraction could be consistent with radio emission from SCOs (i.e., SBHs, NSs). An extended X-ray source (G359.95-0.04), typically interpreted as a pulsar wind nebula, has also been detected (e.g., Zhao et al. 2022). Further evidence for SCO-star binaries comes from X-ray surveys with Chandra and XMM-Newton, which have revealed faint point sources through Fe XXV $K\alpha$ line emission (Wang et al. 2002). Muno et al. (2003, 2005, 2009) and Zhu et al. (2018) cataloged approximately ~ 3500 such sources, which roughly trace the stellar light distribution; however, source confusion within $5''$ of Sgr A* limits the sensitivity to faint objects. (Muno et al. 2005) suggest an overabundance of such systems in the central parsec compared to the region outside of the NSC, in line with expectation from mass segregation (Bahcall & Wolf 1977). These point sources are generally considered X-ray counterparts to SCO-star binaries, and their population is dominated by magnetic Cataclysmic variables (MCVs), i.e., white dwarf–star systems. qLMXBs appear subdominant ($\sim 2\%$), consistent with Hailey et al. (2018), who reported only 12 SBH containing qLMXBs in the Chandra dataset, most centrally concentrated. Consistent with this conclusion, Krivonos et al. (2021) suggested that out of 20 detected GC very faint X-ray transients, 12 likely correspond to qLMXBs.

2.6. Galactic Center pulsars

Pulsars, a distinct class of SCOs, are short-lived, highly magnetized neutron stars emitting periodic radio flashes. From theoretical arguments, there is expected to be $N_{\text{pulsar}} \sim O(0.1 - 10)$ pulsars in the GC (Eatough et al. 2013; Schödel et al. 2020), but so far none have been detected. Such pulsars, if they exist, could probe the potential of Sgr A* with high precision (e.g., Kramer et al. 2004; Cordes et al. 2004; Pfahl & Loeb 2004). Their detection requires deep, high-cadence radio/mm surveys, which are ongoing with Meerkat, ALMA, and soon SKA (e.g., Kramer & Champion 2013; Kramer & Stappers 2015; Eatough et al. 2015; Mus et al. 2022; Frail et al. 2024). Given extensive prior work, pulsars are excluded from this paper's scope.

3. Current detection strategies for compact objects in the optical and infrared bands

Four general pathways for the detection of compact objects exist:

1. Photometric searches,
2. Spectroscopic searches,
3. Astrometric searches,
4. Gravitational lensing searches.

We discuss each of these below.

3.1. Photometric searches

Photometric searches for compact objects generally rely on detecting periodic variability in the light curves of gravitationally bound binary systems. Such variability is caused by the gravitational influence of the companion object, which deforms the primary, modulates its luminosity, and thereby imprints the orbital dynamics on the light curve (e.g., Morris 1985). The strength of the imprinted variability depends on the binary mass ratio, with higher variability amplitude in tighter systems and greater mass ratios (Morris & Naftilan 1993). This variability can be significant, reaching $\sim 20\%$ for heavy, tightly bound systems (Gomel et al. 2021b). However, only the mass ratio, and not the two individual masses, can be derived with photometry. Because ellipsoidal variability arises in both star–star binaries and star–compact object systems (e.g., Moe & Di Stefano 2017; Gomel et al. 2021a), in order to constrain the nature of the unseen secondary object the mass of its luminous companion must be known, but is often highly uncertain. Photometric searches have been greatly enhanced by large catalogs constructed by space observatories such as TESS (Ricker et al. 2015), OGEL (Udalski et al. 2015), and Gaia (Gaia Collaboration et al. 2016), which survey millions of stars for periodic features in their light curves. For instance, Gomel et al. (2021b) presented a catalog of 10956 short-period ($P < 2.5$ d) ellipsoidal binaries, out of which they identified 136 candidate star-SCO binary systems.

3.2. Spectroscopic searches

Spectroscopic searches of SCO-star binary systems are, in principle, similar to photometric searches, but probe periodic variations in the radial velocity of the luminous counterpart instead of its light curve. As in photometric surveys, SCO-star binaries need to be disentangled from the population of common star-star binaries, and are often identified as a by-catch of binary star surveys (e.g., Giesers et al. 2018; Shenar et al. 2022b; Mahy et al. 2022). Such surveys have detected credible candidate systems in massive, single-lined (SB1) or double-lined (SB2) O/B-type binary systems, with typical orbital periods of a few tens of days. For instance, Shenar et al. (2022b) characterized 51 candidate SCO-O/B-star binary systems, out of which they identified one robust O+BH binary system (Shenar et al. 2022a), and two additional high-confidence candidate systems. Although spectroscopic searches provide strong constraints on system masses, the necessity of dispersing the light significantly reduces their efficiency.

3.3. Astrometric searches

Astrometric searches combine the advantages of photometric and spectroscopic approaches, by using photometry as an efficient survey technique and velocity measurements to derive accurate binary system mass measurements. Specifically, the high astrometric accuracy of the Gaia mission (Gaia Collaboration et al. 2016) makes it a promising instrument to identify Star-SCO binary systems (e.g., Breivik et al. 2017; Mashian & Loeb 2017; El-Badry et al. 2021). Although the number of potentially detectable sources is uncertain, high confidence SCO-star binaries have already been detected with Gaia (El-Badry et al. 2023a,b, 2024).

3.4. Gravitational lensing searches

Finally, SCOs can be revealed through the gravitational magnification of a background source, a phenomenon known as microlensing. Originally proposed by Einstein (1936), microlensing enables serendipitous detections of isolated compact objects acting as lenses along with a precise determination of their mass. Modern, optimized surveys such as the Optical Gravitational Lensing Experiment (OGLE; Udalski et al. 2015), Microlensing Observations in Astrophysics (MAO; Sumi et al. 2016) or the Zwicky Transient Facility (ZTF; Masci et al. 2019) routinely detect microlensing events, and the technique has become a prime method for discovering exoplanets, with more than 200 detections to date (e.g., Mroz & Poleski 2023). In principle, lenses of any mass can be detected with this method; however, to date, only a single isolated stellar-mass black hole has been confirmed (Sahu et al. 2022).

4. Detection strategies for Galactic Center SCOs with the ELT

4.1. A simplified Galactic Center model

Photometric, spectroscopic, and astrometric SCO searches generally rely on the presence of a luminous star in a bound star-SCO binary system, while microlensing only requires a luminous background source along the line of sight. It is thus clear that, in order to estimate the detectability of SCOs in the Galactic Center, we need to estimate the luminosity and distribution of all Galactic Center components, i.e., we need to define a baseline model for the Galactic Center. In order to obtain a realistic, albeit approximate distribution of stars, we model the three significant star formation events measured by Schödel et al. (2020). To do so, we use the stellar evolutionary tracks based on the MESA Isochrones & Stellar Tracks (MIST) isochrones (Dotter 2016). To estimate the number of stars, we adopt the Galactic Center mass from (Fritz et al. 2016), and we model all known major star formation events: 80% of mass formed ≈ 10 Gyr ago, 15% of mass formed ≈ 3 Gyr ago, and 5% of mass formed ≈ 250 Myr ago (based on Schödel et al. 2020). In addition, we include the Young Star cluster assuming a cluster mass of $10^4 M_{\odot}$ and an age of 6 Myr (e.g., Bartko et al. 2009; Lu et al. 2013). For simplicity, we adopt a Kroupa Initial Mass Function (IMF; Kroupa 2001) for the stars. Figure 1 shows the resulting Hertzsprung–Russell diagram. The distance modulus and extinction are accounted for in the stellar flux density (y-axis). While we could use the MIST isochrones to estimate the number of stars, white dwarfs (WD), neutron stars (NS), and SBHs, we adopt the numbers from Zhang & Amaro Seoane (2024) and Gravity Collaboration et al. (2024) instead. These authors provide estimates based on much more sophisticated Fokker–Planck modeling and observational constraints of the NSC. For the following estimates, based on their modeling and observations, we assume that 10^7 stars, 5×10^5 WDs, 10^5 NS, and 10^4 SBHs are present in the Galactic Center Nuclear Star Cluster (i.e., within $\approx 30''$ of Sgr A*).

Finally, the number of compact objects residing in binary systems remains poorly constrained. Although observations show that binaries are present—at least within the younger stellar populations of the NSC (see Introduction)—their overall abundance in the GC is governed by several competing processes: the primordial binary fraction, the efficiency with which star–star binaries capture SCOs, and the subsequent evaporation of binaries through dynamical encounters in the dense clus-

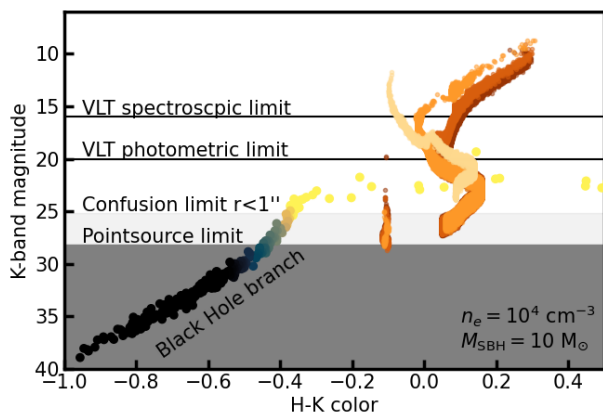


Fig. 1: Model Hertzsprung—Russell diagram of the Galactic Center. Horizontal lines indicate sensitivity limits of the VLT as annotated, shaded regions correspond to the respective ELT/MICADO limits. The orange stellar evolutionary tracks are based on MIST isochrones (Dotter 2016), and use the GC mass reported by Fritz et al. (2016), as well as the age and star formation history reported by Schödel et al. (2020). The light orange track shows the Young Star cluster (von Fellenberg et al. 2022). For all stars, we assume a Kroupa IMF (Kroupa 2001), which may represent a poor approximation in the Galactic Center (e.g., Lu et al. 2013). The annotated, black-to-yellow colored “Black Hole branch” shows the luminosity of modeled SBHs accreting from the Mini-spiral as discussed in subsection 4.6. An artificial scatter of a few percent has been added to the tracks for visualization purposes.

ter environment (for reviews, see Alexander 2005, 2017). Outside the Galactic Center, stars predominantly form in binaries, with the binary fraction increasing strongly with primary mass (e.g., Sana et al. 2013, 2014). Given the top-heavy stellar mass function in the GC ($\alpha \in (-0.45, +1.7)$; e.g., Bartko et al. 2010; Lu et al. 2013; Do et al. 2013; von Fellenberg et al. 2022), one would therefore expect an even higher binary fraction than in the rest of the Milky Way. However, the unusual, disk-like mode of star formation in the GC (e.g., von Fellenberg et al. 2022; Jia et al. 2023) cautions against a straightforward extrapolation of Galactic disk binarity to the NSC. Still, it seems plausible that most stars that ultimately form SBHs and NSs are formed in binary systems.

The stellar density in the GC is too low for binaries to form efficiently through dynamical capture (e.g., Pfuhl et al. 2014). The exchange capture of a more massive component, such as a stellar-mass black hole, by a star-star binary via the Hills mechanism (Hills 1988) is possible, but the rate of such events remains uncertain, as it depends sensitively on the (largely unknown) population of isolated SBHs in the region.

Still, the fact that binaries are observed in the Galactic Center (e.g., Pfuhl et al. 2014, and see Introduction) demonstrates that they do form and can survive for at least part of their evolutionary history. Once formed, binaries interact with both the surrounding NSC and the central SMBH. Repeated two-body encounters tend to drive their evolution toward either coalescence or evaporation (e.g., Alexander 2005). Coalescence timescales for hard binaries are long (comparable to the local relaxation time, i.e., $\sim 10^9\text{--}10$ yr, e.g., Merritt et al. 2010). In contrast, evaporation timescales can be much shorter and depend sensitively on the distance from the SMBH, the binary semi-major axis, and

the masses of both the binary components and the surrounding cluster stars (Pfuhl et al. 2014; Alexander & Pfuhl 2014).

Massive binaries, the progenitors of SBHs, are generally stable over their stellar lifetimes. However, once the SBHs-star binary system forms, even relatively tight systems ($a_0 < 1$ AU) are expected to evaporate over the lifetime of the NSC (~ 10 Gyr, e.g., Pfuhl et al. 2014; Marklund et al. 2025). Recent estimates by Dodici et al. (2026) suggest that all but the most tightly bound binaries [$a_0(r > 1 \text{ pc}) < 1 \text{ AU}$ and $a_0(0.01 \text{ pc} < r < 0.1 \text{ pc}) < 0.01 \text{ AU}$] will evaporate within 10^{10} yr. This implies that the oldest and most numerous stellar populations in the NSC ($\sim 80\%$) are unlikely to retain a significant binary fraction. Nevertheless, a non-negligible fraction of binaries may persist among the more recently formed stars ($\sim 20\%$).

Finally, SBHs can grow substantially in mass via mergers (e.g., Doctor et al. 2020; The LIGO Scientific Collaboration et al. 2025). NSCs are of particular interest in this context as the dense stellar fields allow for multiple pathways for SCOs to merge and form heavier merger products (e.g., Hoang et al. 2018; Kremer et al. 2020). For instance, by explicitly modeling the merger product population in the Galactic Center, Newton et al. (2026) find that SBHs can reach masses of up to $\sim 200 M_{\odot}$ and predict the presence of several tens of such objects. They estimate that although more massive products may form, they efficiently sink and merge with Sgr A* and are therefore only transiently present.

Given these uncertainties and the simplified NSC model adopted here, we do not attempt to derive a detailed or self-consistent binary fraction. Instead, we account only for the plausible presence of binaries. As discussed in subsection 2.3, we note that Chen et al. (2023) derive a substantially different star formation history, and importantly derive an estimate of about an order of magnitude larger for the number of SBHs present in the Galactic Center (2.5×10^5). They also model the SBH-SBH binary fraction explicitly, and estimate the presence of 2.2×10^4 SBH-SBH binaries, but do not report a SCO-star-binary fraction. We show in what follows that under any circumstances only a small fraction of the SCOs are likely detectable in the Galactic Center, thus such an increased SBHs population would trivially correspond with a larger number of detectable systems.

4.2. ELT/MICADO observations of the Galactic Center

The Extremely Large Telescope (ELT) is the flagship ground-based optical and near-infrared observatory of the European Southern Observatory (ESO), currently under construction on Cerro Armazones in northern Chile (ESO 2024). With a 39 m diameter segmented primary mirror, the ELT will provide an unprecedented combination of light-gathering power and angular resolution, enabling advances across stellar astrophysics, galaxy formation, and fundamental physics (e.g., Gilmozzi & Spyromilio 2007). The telescope is designed to operate in conjunction with advanced adaptive optics systems, allowing it to achieve diffraction-limited performance at near-infrared wavelengths (e.g., Bonnet et al. 2018). One of the ELT’s first-light instruments is MICADO (Multi-Adaptive Optics Imaging Camera for Deep Observations), a high-resolution near-infrared imager optimized for precision astrometry and deep imaging (Davies & Genzel 2010; Davies et al. 2021; Sturm et al. 2024). At first, MICADO will operate using a single-conjugate natural guide star adaptive-optics system (SCAO) system developed by the MICADO and MAORY consortia, and will subsequently be upgraded to operate behind the multi-conjugate adap-

tive optics module MAORY, which delivers uniform, high-Strehl imaging over fields of view up to $\sim 1'$ (Diolaiti et al. 2016).

MICADO observations of the Galactic Center will be transformative because they overcome or greatly reduce the two main obstacles limiting 10-m-class telescope observations. First, the high spatial resolution of ~ 10 mas in the K-band greatly reduces confusion in the Galactic Center. While the stellar density in the central arcsecond of 10^4 stars/as² still implies confusion-limited observations for the central few arcseconds, the surface density of stars drops off steeply with distance and thus outside of the central arcsecond the observations should be limited by integration time. This picture is complicated by the presence of several very bright stars, specifically IRS7 ($K_{\text{mag}} \approx 7$ mag; e.g., Ott et al. 1999) and the IRS16 sources ($K_{\text{mag}} \approx 10 \dots 12$ mag; e.g., Martins et al. 2007) which will likely limit observations in their immediate spatial vicinity (which includes Sgr A*). This may require specific mitigation strategies such as a field stop, and excellent AO-performances over a large field of view (FOV). Assuming these technical limitations can be overcome, photometric sensitivities should range from $K_{\text{mag}} = 25$ in the confusion-limited central arcsecond and approach $K_{\text{mag}} = 29$ at larger projected distances for a typical, July/August observation of the Galactic Center ($t_{\text{obs}} \approx 6$ h, Davies et al. 2021). These limits are indicated by light and dark gray shaded regions in Figure 1. Finally, MICADO will have excellent relative astrometry, allowing for $\sim 50 \mu\text{s}$ precision during a typical good observing night (Davies et al. 2021).

4.3. Photometric detection of SCO-star systems in the Galactic Center

Photometric detection of SCOs, i.e., the identification of ellipsoidal binaries, requires the presence of a luminous companion star. Importantly, the ELT will allow for the detection of the G- and K-type stars that typically represent host stars in known Low-Mass X-ray Binaries (LMXBs), composed of a main-sequence star and an SCO. To illustrate the detectability of such a system, it is useful to study a known LMXB in which the stellar system is well-characterized, and scale its luminosity to the Galactic Center distance. For instance, in the case of XTE J1118+480, the host star is a K7V main sequence star, with a K-band magnitude of $K_{\text{mag}} \sim 16.7$, $\Delta K_{\text{mag}} \sim 0.3$, and a photometric period of $P \sim 53$ d (Gelino et al. 2006). If this system was placed in the Galactic Center, the host star would have a minimum magnitude of $K_{\text{mag}} \sim 23.6$, see Figure 2. Although the error bars were artificially imposed on the data (assuming 10% photometric noise), it is evident that such a system would be readily detectable by the ELT within a year, provided the Galactic Center is monitored on a semi-regular basis ($\sim 1/\text{month}$), as is routinely done today with the VLT. This discussion illustrates that, in principle, the detectability of such systems is not inherently difficult and requires only moderately regular cadence observations, comparable to those conducted in the Galactic Center over the past two decades. At the same time, even very conservative (i.e., $\sim 1\%$) estimates of the binary fraction in the Galactic Center predict the presence of $\sim 10^5$ ordinary star–star binary systems, which constitute a significant astrophysical (rather than instrumental) noise source in the identification of SCO–star binaries.

It is therefore evident that addressing this problem demands survey-scale analysis strategies that have not yet been systematically applied to the Galactic Center. Nevertheless, constraining the photometric binary population across the entire stellar content of the Galactic Center, independent of the nature of the com-

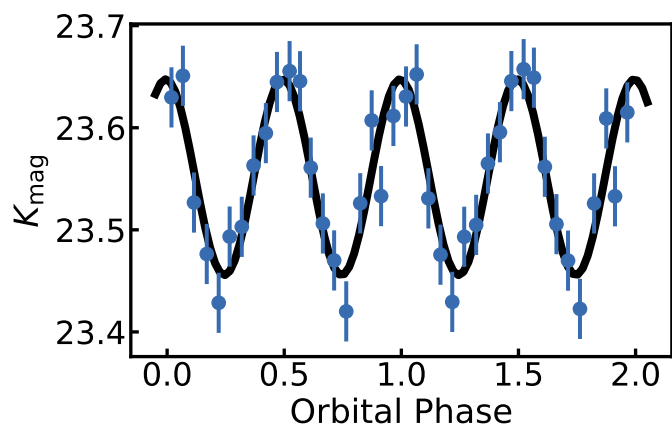


Fig. 2: Mock observations of the variability of the host K7V main sequence star in the LMXB XTE J1118+480, scaled as if it were located in the Galactic Center. The star has a K-band magnitude ~ 23.6 , which is readily detectable by the ELT (Gelino et al. 2006), assuming a constant extinction of $A_K = 2.42$ for simplicity. There are differences in star flux density of a factor $\times 10$ between references (i.e., Plotkin et al. 2015), but the system is readily detected in any case. We have assumed 10% photometric uncertainty.

panion object, represents an obvious and compelling research direction for the upcoming ELT era. The eventual detection of elusive star–SCO candidate systems may well be its most rewarding outcome.

4.4. Spectroscopic detection of SCO-star systems in the Galactic Center

MICADO is currently only envisioned to offer a slit spectrometer. Due to the extreme confusion in the Galactic Center, slit spectrometry is inefficient for survey style searches and can only be used to track a known, bright star (such as S2). Therefore, while individual promising and bright enough candidate star–SCO systems maybe followed spectroscopically, systematic spectroscopic searches will have to wait for Integral Field Unit (IFU) instruments such as HARMONI (Thatte et al. 2021) or ANDES (Marconi et al. 2024), and we defer the details to future work.

4.5. Astrometric detection of SCO-star systems in the Galactic Center

The last few years have illustrated that, thanks to the astrometric precision of the Gaia mission, astrometric detection of compact objects is both feasible and robust (e.g., El-Badry et al. 2023b,a, 2024). Gaia achieved astrometric accuracies $\sim 20 \mu\text{s}$ in its third data release (Gaia Collaboration et al. 2023). The ELT/MICADO will achieve a comparable (relative) astrometric accuracy of $\sigma_{\text{MICADO}} \approx 50 \mu\text{s}$ (Massari et al. 2016; Davies et al. 2021). At a distance of 8.2 kpc, this corresponds to a projected spatial scale of ~ 0.4 AU.

To demonstrate the feasibility of astrometric SCO-star detections, we use an observed example: a black hole discovered in a sun-like star system (El-Badry et al. 2023b). This system, discovered in the Gaia astrometry and radial velocity sample, consists of a G-type star primary and is found at distance of 480 pc. The hidden black hole companion has a mass of $9.62 M_{\odot}$.

Comparing with Figure 1, it is clear that the host star (flux density ~ 22 mag) would be readily detectable if it were located in the Galactic Center. The system has a semi-major axis of 1.40 ± 0.01 AU and an orbital period of $P \approx 185$ d. Using Thiele-Innes elements (e.g., Breivik et al. 2017) and the orbital parameters reported in El-Badry et al. (2023b), we project the system as if it were observed in the Galactic Center (Figure 4). We use a realistic observing cadence of three images per month over five years, and assume a nominal uncertainty of $50 \mu\text{as}$. Figure 4 shows that such a measurement is feasible, and robust measurements of the system’s orbit would be available after a few years.

Next, we try to estimate the number of SCO-star binaries that could be detected with MICADO. For the purpose of this calculation, we assume a binary fraction of 50%, yielding 5000 binary systems based on the assumption of 10^4 SBHs within $\approx 30''$. This assumption, while somewhat arbitrarily, is consistent with the high binary fraction of massive stars (e.g., Sana et al. 2013). Additional binaries may be formed by tidal capture, but these are expected to be a small fraction of the population (Generozov et al. 2018). Because the total number of binaries in the GC is poorly constrained (e.g., Gautam et al. 2019), we do not attempt to obtain an absolute estimate of detectable systems; instead we derive a fractional estimate. The binary orbital properties are adopted from Dodici et al. (2026), who demonstrated that a significant fraction of initially wide binaries evolve into near-contact systems through von Zeipel–Lidov–Kozai (ZLK) oscillations. They further report a radial dependence of the binary semi-major axis. For the purpose of this calculation, we use their semi-major axis distribution for two radial bins: 0.1 pc to 1 pc and > 1 pc. We further assume a thermal eccentricity distribution and a black hole mass of $10 M_{\odot}$, while we adopt the stellar mass distribution from subsection 4.1 and use Thiele-Innes elements to calculate the projected orbits. Under these assumptions, we find that approximately $\sim 15\%$ of the SCO-star binaries exhibit orbital variations large enough to be detectable astrometrically at the $3\sigma = 1.2$ AU level. If instead we assume that the binary orbits are circular, this estimate is not significantly altered ($\sim 18\%$ detected). Furthermore, we emphasize that our fractional estimate for detectability is independent of the assumed total number of systems; it depends only on their orbital properties.

Figure 3 presents the resulting distributions for star-SCO binaries, along with a representative sample of orbits for which astrometric detections should be feasible. Of course, this estimate is highly uncertain, as neither the fraction of stellar compact objects (SCOs) bound in binary systems nor their orbital properties are well constrained. Specifically, the total number of detectable systems is a function of the binary fraction, and the percentage of detectable stars sensitively depends on the binary semi-major axes distribution. If the binary semi-major axis is too small, that system will not be detectable; the calculations by Dodici et al. (2026) indicate that this might be the case at radial separations from Sgr A* smaller than ~ 0.1 pc ≈ 2.5 arcseconds, where the fraction of detectable binaries drops to $\sim 1\%$. On the other hand, Dodici et al. (2026) focus only on the main-sequence phase of stellar binaries and do not account for modifications occurring during later evolutionary stages. These later stages, such as the common-envelope phase, are expected to significantly alter the binary orbital parameters (e.g., Soberman et al. 1997). If this radial dependence of the binary semi-major axis is correct, it would also mean that both photometric and astrometric methods have complementary sweet-spot regimes. Specifically, this occurs because closer to Sgr A*, near-contact binaries with strong photometric variability are more common, while at fur-

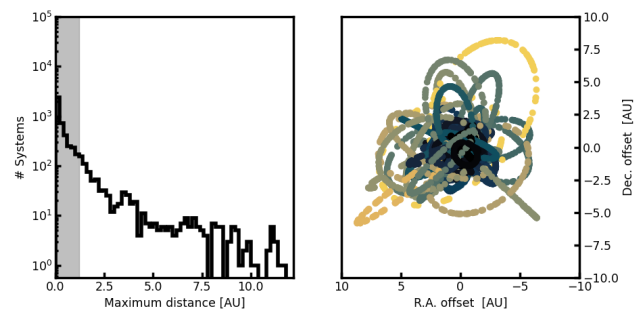


Fig. 3: Left: Maximum size of orbital ellipses for simulated star-SCO binaries using the semi-major axis distributions in Dodici et al. (2026) as input. The gray shaded region shows the $\geq 3\sigma$ detection limit assuming $50 \mu\text{as}$ astrometric uncertainty. Right: 100 sample orbits for binaries that would be detectable with high significance.

ther distances larger semi-major axis systems are more easily detected via astrometric means. In addition to the unknown properties of the SCO-star binaries, we neglect the uncertainty stemming from subtracting the intrinsic proper motion of the system, which, bound to Sgr A*, should experience linear drifts on the order of a few mas/yr. While this uncertainty is certainly relevant for the first few years, proper motion solutions should be well constrained after a few years. More critical is astrometric confusion, which, given the extremely large number of stars in the Galactic Center, will be a limiting factor (Fritz et al. 2010). Due to its transient, stochastic nature, and the unknown stellar distribution and effective AO-performance of MICADO in the Galactic Center, assessing its impact is beyond the scope of this work.

4.6. Direct detection of SCOs in the Galactic Center

4.6.1. White dwarfs

As indicated in Figure 1, almost all WDs in the GC should be detectable photometrically with ELT/MICADO, and their detection is facilitated by color measurements. Specifically, their detectability requires precision color measurements with $\delta H - K < 0.1$, which has been challenging with VLT data (e.g., Buchholz et al. 2009; Nogueras-Lara et al. 2018; Schödel et al. 2020; Gallego-Cano et al. 2024). For instance, while in some cases color-based star classifications have been spectroscopically confirmed, this has only been successful for brighter stars (i.e., $m_K < 15 \dots 16$; Gallego-Cano et al. 2024). Specifically, while photometric sensitivities are typically on the order $\sim 0.01 \dots 0.1$ mag, color measurements are systematically limited by stellar confusion and spatially variable extinction. The ELT will eliminate or at least significantly reduce stellar confusion as source of systematic uncertainty. Still, the spatially variable extinction remains an issue, and it is typically on the order of $\delta A_{\lambda} \sim 0.2$ mag (e.g., Schödel et al. 2010; Fritz et al. 2011; Nogueras-Lara et al. 2018). At the same time, the ELT will increase the number of detectable stellar sources by a factor of $10^3 - 10^4$, thereby enabling substantially improved stellar-based extinction measurements. The challenge of identifying WDs against the noisy extinction (and confusion) foreground then becomes a well-posed classification problem, where classification models based on our theoretical understanding of stellar evolution are very robust. It may thus be possible to achieve high

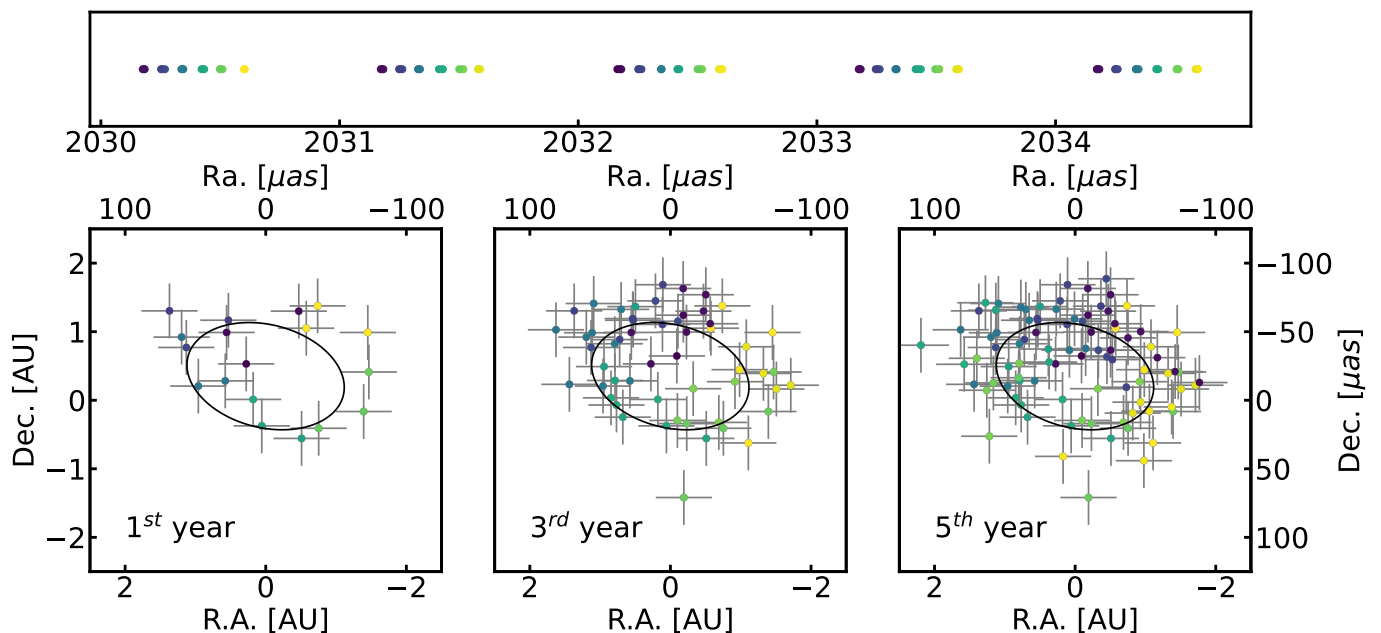


Fig. 4: Mock astrometric observation of the Gaia-detected star-stellar mass black hole binary system (El-Badry et al. 2023b) if it were located in the Galactic Center. We scale the orbital elements to the distance of the Galactic Center (black solid line), assume a regular observing cadence during the Galactic Center season (top panel, color indicates observing month), and an astrometric accuracy of $50\mu\text{as}$. For simplicity, we assume perfect subtraction of the proper motion of the binary in the Galactic Center potential, and neglect astrometric confusion (which can occur if the system crosses paths with another star).

enough photometric performance to reliably detect GC WDs, although a dedicated study of this is beyond the scope of this work.

In addition to normal WDs, $\sim 1\%$ of WDs show an infrared excess (e.g., Madurga Favieres et al. 2024), most likely caused by a warm debris accretion disk. These systems show significant mid-infrared excess, but their K and H band behavior is much less known. Still, given their typical luminosities of ~ 16 mag in the WISE W1 filter ($\lambda = 3.3\ \mu\text{m}$) they may form a significant, bright, odd-colored species in the H-R diagram.

4.6.2. Stellar black holes

The Galactic Center hosts an estimated $\approx 10^4$ stellar black holes (Zhang & Amaro Seoane 2024) within the central parsec, which appear to be largely “dormant” and have mostly evaded detection. Yet, even isolated BHs may accrete from the gas-rich environment, with accretion states plausibly resembling those of Sgr A*. Significant ionized and molecular gas is present (see Figure 5), most prominently in the mini-spiral, a system of gas clouds ($n_{\text{gas}} = 2 - 21 \times 10^4\ \text{cm}^{-3}$) orbiting around the central MBH (e.g., Zhao et al. 2009, 2010). Moreover, several tens of Wolf-Rayet stars exist (Paumard et al. 2006; Lu et al. 2006; von Fellenberg et al. 2022; Jia et al. 2023, e.g.), whose strong winds likely enhance accretion, and are thought to power the present-day activity of Sgr A* (e.g., Quataert 2004; Cuadra et al. 2008; Shcherbakov & Baganoff 2010; Calderón et al. 2020; Ressler et al. 2020b). In this subsection we address the important question: how bright would a stellar black hole be if it accreted from any of those gas sources?

The luminosity of a black hole can be estimated as a fraction of the so-called Eddington luminosity $L_{\text{Edd}} \propto M_{\text{BH}}$ [or equivalently, the Eddington accretion rate, $\dot{m}_{\text{Edd}} = L_{\text{Edd}}/(\eta c^2)$, where η is the radiative efficiency and c is the speed of light]. Given Sgr A*'s luminosity of $\sim 10^{35}\ \text{erg s}^{-1}$, a stellar-mass black hole

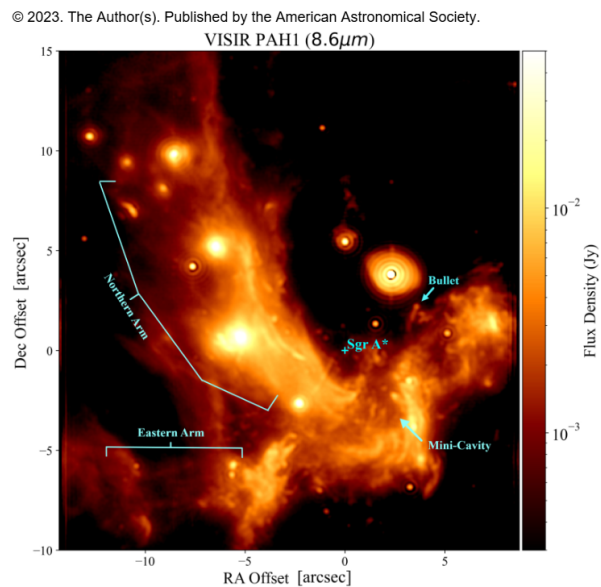


Fig. 5: Paschen- α image of the central ~ 15 arcseconds² of the galaxy, showing the large-scale mini-spiral gas streamers. The image was published in Dinh et al. (2024).

with $M_{\text{BH}} = 10 M_{\odot}$ accreting at a comparable fraction of Eddington would plausibly have a luminosity of $L_{\text{SCO}} \sim 10^{30}\ \text{erg s}^{-1}$, which is roughly an order of magnitude larger than the ELT detection limit in the Galactic Center [$O(10^{29}\ \text{erg/s})$].

However, relevant for the detectability is the peak frequency at which most of the emission is radiated. Since the emission mechanism for low-luminosity accretion flows is typically synchrotron radiation, this peak frequency is given by the criti-

cal frequency of ν_b . Low accretion rates lead to a so-called Radiatively Inefficient Accretion Flow (RIAF) state, for which $\nu_b \propto M_{\text{BH}}^{1/2} \cdot \dot{m}^{-1/2}$ (where M_{BH} is the SBH mass and \dot{m} is the accretion rate, e.g., Pesce et al. 2021). This dependence implies that there exists a regime of black hole masses and accretion rates for which the synchrotron emission peaks in the NIR; as illustrated in the right panel Figure 6, this sweet-spot regime is for SBHs with mass ranges between $10 \dots 100 M_{\odot}$. We have used the LLAGN code by Pesce et al. (2021) to compute the SEDs.

The accretion rate of an SBH that accretes as it moves through the surrounding material can be estimated using the Bondi-Hoyle-Lyttleton accretion formalism (e.g., Hoyle & Lyttleton 1939; Bondi & Hoyle 1944; Edgar 2004), where the mass accretion rate is given by (e.g., Fujita et al. 1998)

$$\begin{aligned} \dot{m} &\propto \pi r_{\text{cap}}^2 \rho_{\text{gas}} V \\ &\approx 7.4 \times 10^{13} \left(\frac{M}{M_{\odot}} \right)^2 \left(\frac{n_{\text{gas}}}{10^2 \text{ cm}^{-3}} \right) \left(\frac{v_{\text{eff}}}{10 \text{ km s}^{-1}} \right)^{-3} [\text{g s}^{-1}], \end{aligned} \quad (2)$$

where v_{eff} is the effective velocity of the gas and the black hole, i.e., $v_{\text{eff}} = \sqrt{v_{\text{BH}}^2 + c_s^2}$, where v_{BH} is the relative velocity of the black hole to the surrounding medium and c_s is the sound speed. For typical Galactic Center ionized gas temperatures (10^4 K ; Genzel et al. 2010) the sound speed is negligible $c_s = 11.7(T/10^4 \text{ K})^{1/2} \text{ km s}^{-1} \approx 10 \text{ km s}^{-1}$ (Wang & Loeb 2014), setting a lower limit for v_{eff} , while typical Keplerian velocities are $V \sim \mathcal{O}(10^2 \text{ km s}^{-1})$ (e.g., Genzel et al. 2003).

However, it is well known that for RIAFs, only a fraction of the gas accreted reaches the event horizon because most of it is lost in the form of outflows. For instance, in the case of Sgr A*, only 0.01% of the gas accreted at the Bondi radius reaches the black hole event horizon. In general, this result is seen in both simulations and observations of RIAF accretion flows regardless of the physical scale of the system (Xu & Stone 2019; Gillessen et al. 2019), whether or not the flow is magnetized (Ressler et al. 2018, 2020a), whether or not the flow has significant angular momentum (Pen et al. 2003; Pang et al. 2011; Ressler et al. 2021; Galishnikova et al. 2025; Cho et al. 2023), and for several different feeding mechanisms (Ressler et al. 2023; Guo et al. 2024; Labaj et al. 2025). Xu (2023) argue that the significant reduction of the large-scale accretion flow is, in fact, a general property of hot, turbulent accretion, and predict $\dot{m}(r_B) \propto r^{-0.5 \dots 1}$ (consistent with the simulations). Recently, Lalakos et al. (2025) performed large scale simulations of Bondi-like accretion onto black holes, for which they claim universality. In these simulations, they find Bondi-radius-to-horizon-scale accretion scaling

$$\dot{m}(r_B) = (1.0 \pm 0.2) \times 10^{-3} \left(\frac{r_B}{10^5 r_g} \right)^{-0.66 \pm 0.03} [\dot{m}_{\text{Bondi}}], \quad (3)$$

where \dot{m}_{Bondi} is given as in Equation 2, and r_B and r_g is the Bondi and gravitational radius. Here, we have used their relation for Magnetically Arrested Disks (MADs), which is the leading model for Sgr A* (e.g., Ressler et al. 2020b; Event Horizon Telescope Collaboration et al. 2022) and likely a common black hole accretion state for RIAFs (Zamaninasab et al. 2014; Chael et al. 2019; Event Horizon Telescope Collaboration et al. 2019; Liska et al. 2020).

The left panel of Figure 6 illustrates that SBHs can be detected if they move with and accrete from one of the gas-dense

structures like the mini-spiral. Thus, direct constraints on the orbital distribution of SCOs are within reach of the ELT/MICADO. As illustrated in Figure 1, the actual detection of such SBHs is facilitated by their color, since their synchrotron emission would have a substantially different spectral index than the black-body emitting stars. Important caveats apply to the scaling relations found by Lalakos et al. (2025), most importantly that they do not explore the impact of different magnetizations of the accreting gas, which is expected to be high in the Galactic Center (e.g., Eatough et al. 2013). Additionally, they assume spherical / free-fall accretion on the SBH, that is that the gas does not possess angular momentum, which is likely important for orbiting SBHs. Finally, their work does not account for radiative cooling, which would be non-negligible for the initially cold and dense gas accreting from the mini-spiral, even if the flow ultimately remains in the RIAF regime. Upcoming work by Labaj et al. aims to model such systems in an MHD framework to better constrain the accretion onto SBHs embedded in the mini-spiral environment.

To estimate the number of stellar-mass black holes (SBHs) that could be detected with MICADO on the ELT, we first determine their effective velocity relative to the mini-spiral. For the underlying geometry, we adopt the three-dimensional structure of the mini-spiral derived from the orbital elements measured by Nitschai et al. (2020). Since the intrinsic width of the mini-spiral is not known, we can only place upper limits based on its projected width of approximately (2–5 arcsecond, see Figure 5). We then construct a simulated dark cluster of SBHs, modeled as an isotropic distribution following a power-law density profile $n_{\text{SBH}} \propto r^{1.5}$ (Zhang & Amaro Seoane 2024), with a total population of $n_{\text{SBH}} = 10^4$ (GRAVITY Collaboration et al. 2022). The resulting distributions are illustrated in Figure 7.

Given our assumptions, we estimate that a few tens of black holes will be above the nominal detection limit – by up to a factor 10^2 . Because the spatial distribution of SBHs, the true width of the mini-spiral, the SBH mass function, and the total population remain poorly constrained, this estimate based on our derived luminosity distributions is speculative. Still, our assumptions are relatively conservative, as we have chosen a single mass of $10 M_{\odot}$ for the putative SBHs, and ignored the possibilities that they have experienced mergers or significant accretion during their lifetime. Heavier black holes will be significantly brighter because of the $\dot{m} \propto M_{\text{BH}}^2$ dependence of accretion. Furthermore, our assumption that the mini-spiral is a very small three-dimensional structure of ~ 1 arcseconds is highly conservative, as Figure 5 seems to indicate that the mini-spiral is significantly larger. If we were to use less conservative, more realistic assumptions about the size of the mini-spiral, then we would estimate that $\mathcal{O}(10^2)$ detectable SBHs. Of course, in any case, the most critical assumption of the actual presence of a dark cluster of $\sim 10^4$ SBHs needs to be fulfilled.

5. Conclusions

In this paper, we demonstrate that the Galactic Center dark cluster — the cluster of stellar compact objects bound to Sgr A* — can, in principle, be observationally constrained. We demonstrate three different, complementary paths to detection. Photometric detection via stellar ellipsoidal variability, astrometric detection via the orbital astrometric signature of the dark-component in star-SCO binaries, and finally, direct detection of isolated, accreting SBHs. A fourth pathway, via microlensing events of background stars, is photometrically simple, but dedicated surveys are too costly to implement and thus detecting

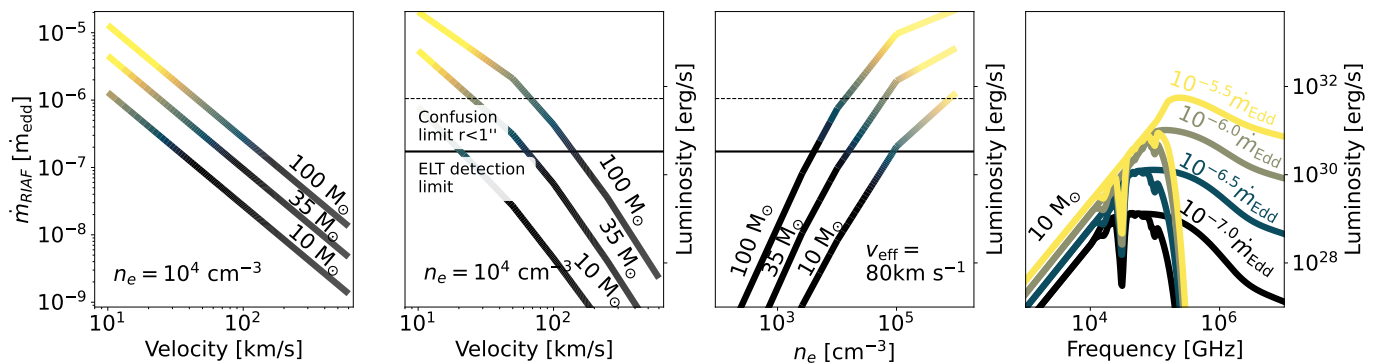


Fig. 6: Left panel: Accretion rate in Eddington units for a $10 M_{\odot}$ black hole based on scaling relations in Lalakos et al. (2025), appropriate for radiatively inefficient, turbulent flows. Center two panels: Luminosity of accreting SBHs for different mass ranges, different effective velocity (left center) and different number density of the accreting gas (right center); the color encodes the accretion rate as indicated by the curves in the leftmost panel. The solid horizontal line indicates the ELT detection limit while the dashed horizontal line indicates the confusion and photometric sensitivity multiplied by the extinction factor. Right panel: Model SEDs of a $10 M_{\odot}$ SBH for different accretion rates computed using the model by Pesce et al. (2021). The smoother lines do not include the effects of extinction, while the more irregular curves do based on the extinction law by Fritz et al. (2011).

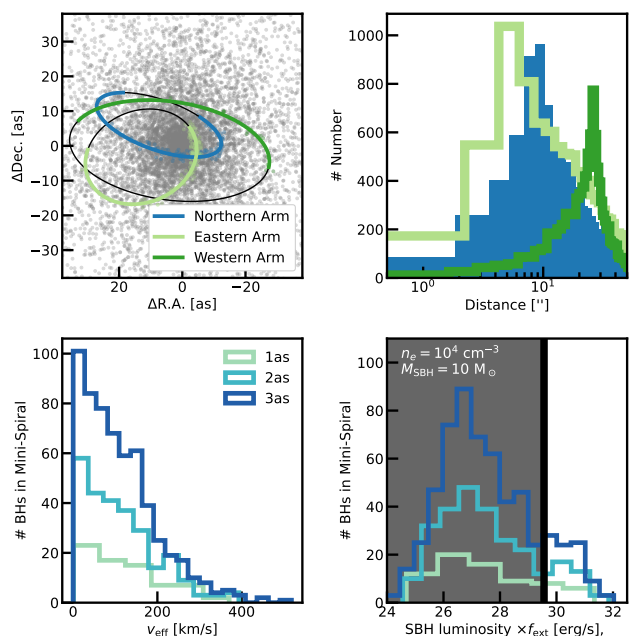


Fig. 7: Top left panel: Spatial distribution of SBHs in our model, where SBHs within 1 arcsecond of the best fit orbits of the three mini-spiral arms are highlighted with the respective colors. Top right panel: Histogram showing the distances from the respective best-fit mini-spiral orbits. Bottom left panel: Number of SBHs as a function of effective velocity for three different, assumed mini-spiral widths. Bottom right panel: Respective luminosities of the SBHs, where we have assumed a conservative black hole mass of $10 M_{\odot}$ and a density of 10^4 cm^{-3} for the accretion scaling laws by Lalakos et al. (2025); the shaded gray region indicates objects to faint too be detectable.

these events can only occur by chance. Our paper adopts optimistic assumptions about instrument performance, and crucially requires overcoming bright-star confusion in the crowded, luminous, Galactic Center. Most importantly, we do not discuss how to identify these exotic objects in the $O(10^7)$ stars that re-

side in the Galactic Center from a practical observational standpoint, which is much more complicated than achieving a high enough signal-to-noise ratio (which we have estimated in this paper). This science case is somewhat auxiliary to the obvious case to study the mass, dynamics, and evolutionary state of the Galactic Center with the ELT/MICADO. Given its recently challenged star formation history (Chen et al. 2023), it is clear that a complete and a sufficiently accurate measurement of the stellar properties of the NSC (e.g., Figure 1) is of central importance to some of the most pressing questions in astronomy, such as what the expected extreme-mass ratio inspiral rate could be for LISA sources (e.g., Amaro-Seoane et al. 2017), whether or not there could be local foreground gravitational wave signals (e.g., Xuan et al. 2024; Amaro Seoane & Zhao 2025), and/or how the galaxy and supermassive black hole have coevolved over time (e.g., Volonteri 2010; Chen et al. 2023). With first closure of the ELT-dome structure, and the completion of the MICADO cryogenic chamber already achieved, this paper demonstrates that the time to prepare Galactic Center observations in the ELT era has come. The extreme amount of data that needs to be processed (by Galactic Center community standards), manipulated, and analyzed, calls for timely preparation. The problem is difficult, but the prize is high.

Acknowledgements. We thank our referee, Mark Morris, for a thorough review and comments that substantially contributed to the manuscript. SDvF thanks Mark Morris and Gunther Witzel for the fruitful discussions on the Galactic Center dark cluster. SDvF gratefully acknowledges the support of the Alexander von Humboldt Foundation through a Feodor Lynen Fellowship and thanks CITA for their hospitality and collaboration; and is grateful for scientific input on the manuscript to Reinhard Genzel, Frank Eisenhauer, Stefan Gillessen, and all members of MPE GC team. We thank Michal Zajaček and Aris Lalakos for the discussion on radiatively inefficient accretion onto compact objects. We thank Mark Dodici for the insightful discussions on Galactic Center binary star properties; and Aleksey Generozov on the help implementing and understanding the stellar evolutionary track models. This manuscript was prepared with the assistance of an AI-based large language model (Microsoft Copilot, GPT-5 family) for language editing and Python code generation. The authors take full responsibility for the scientific content, data analysis, and interpretation presented in this work. All code was reviewed, validated, and executed by the authors. SDvF and SMR acknowledge the support of the Natural Sciences and Engineering Research Council of Canada (NSERC), [funding reference number 568580] Cette recherche a été financée par le Conseil de recherches en sciences naturelles et en génie du Canada (CRSNG), [numéro de référence 568580]. SDvF is supported by the Canadian Space Agency (23JWGO2A01). ML acknowledges the GACR Junior Star grant no. GM24-10599M for support.

References

- Alexander, T. 2005, *Phys. Rep.*, 419, 65
- Alexander, T. 2017, *ARA&A*, 55, 17
- Alexander, T. & Hopman, C. 2009, *ApJ*, 697, 1861
- Alexander, T. & Pfuhl, O. 2014, *ApJ*, 780, 148
- Amaro-Seoane, Gair, J., Freitag, M., et al. 2007, *Classical and Quantum Gravity*, 24, R113
- Amaro-Seoane, P., Aoudia, S., Babak, S., et al. 2012, *Classical and Quantum Gravity*, 29, 124016
- Amaro-Seoane, P., Audley, H., Babak, S., et al. 2017, arXiv e-prints, arXiv:1702.00786
- Amaro-Seoane, P. & Zhao, S.-D. 2025, *J. Cosmology Astropart. Phys.*, 2025, 015
- Bahcall, J. N. & Wolf, R. A. 1976, *ApJ*, 209, 214
- Bahcall, J. N. & Wolf, R. A. 1977, *ApJ*, 216, 883
- Bartko, H., Martins, F., Fritz, T. K., et al. 2009, *ApJ*, 697, 1741
- Bartko, H., Martins, F., Trippe, S., et al. 2010, *ApJ*, 708, 834
- Blum, R. D., Ramírez, S. V., Sellgren, K., & Olsen, K. 2003, *ApJ*, 597, 323
- Boehle, A., Ghez, A. M., Schödel, R., et al. 2016, *ApJ*, 830, 17
- Bondi, H. & Hoyle, F. 1944, *MNRAS*, 104, 273
- Bonnet, H., Biancat-Marchet, F., Dimmler, M., et al. 2018, in *Society of Photo-Optical Instrumentation Engineers (SPIE) Conference Series*, Vol. 10703, *Adaptive Optics Systems VI*, ed. L. M. Close, L. Schreiber, & D. Schmidt, 1070310
- Bower, G. C., Deller, A., Demorest, P., et al. 2014, *ApJ*, 780, L2
- Bower, G. C., Markoff, S., Dexter, J., et al. 2015, *ApJ*, 802, 69
- Bower, G. C., Roberts, D. A., Yusef-Zadeh, F., et al. 2005, *ApJ*, 633, 218
- Breivik, K., Chatterjee, S., & Larson, S. L. 2017, *ApJ*, 850, L13
- Buchholz, R. M., Schödel, R., & Eckart, A. 2009, *A&A*, 499, 483
- Burkert, A., Gillessen, S., Lin, D. N. C., et al. 2024, *ApJ*, 962, 81
- Calderón, D., Cuadra, J., Schartmann, M., Burkert, A., & Russell, C. M. P. 2020, *ApJ*, 888, L2
- Chael, A., Narayan, R., & Johnson, M. D. 2019, *MNRAS*, 486, 2873
- Chatterjee, K., Mondal, S., Palit, B., et al. 2025, *ApJ*, 992, 210
- Chatzopoulos, S., Fritz, T. K., Gerhard, O., et al. 2015, *MNRAS*, 447, 948
- Chen, Z., Do, T., Ghez, A. M., et al. 2023, *ApJ*, 944, 79
- Cho, H., Prather, B. S., Narayan, R., et al. 2023, *ApJ*, 959, L22
- Cordes, J. M., Kramer, M., Lazio, T. J. W., et al. 2004, *New A Rev.*, 48, 1413
- Cuadra, J., Nayakshin, S., & Martins, F. 2008, *MNRAS*, 383, 458
- Davies, R. & Genzel, R. 2010, *The Messenger*, 140, 32
- Davies, R., Hörmann, V., Rabien, S., et al. 2021, *The Messenger*, 182, 17
- Dinh, C. K., Ciurlo, A., Morris, M. R., et al. 2024, *AJ*, 167, 41
- Dioliati, E., Ciliegi, P., Abicca, R., et al. 2016, in *Society of Photo-Optical Instrumentation Engineers (SPIE) Conference Series*, Vol. 9909, *Adaptive Optics Systems V*, ed. E. Marchetti, L. M. Close, & J.-P. Véran, 99092D
- Do, T., Lu, J. R., Ghez, A. M., et al. 2013, *ApJ*, 764, 154
- Do, T., Witzel, G., Gautam, A. K., et al. 2019, *Astrophysical Journal*, 882, L27
- Doctor, Z., Wysocki, D., O’Shaughnessy, R., Holz, D. E., & Farr, B. 2020, *ApJ*, 893, 35
- Dodici, M., Tremaine, S., & Wu, Y. 2026, *ApJ*, 1000, 226
- Dotter, A. 2016, *ApJS*, 222, 8
- Eatough, R., Lazio, T. J. W., Casanellas, J., et al. 2015, in *Advancing Astrophysics with the Square Kilometre Array (AASKA14)*, 45
- Eatough, R. P., Falcke, H., Karuppusamy, R., et al. 2013, *Nature*, 501, 391
- Edgar, R. 2004, *New A Rev.*, 48, 843
- Einstein, A. 1936, *Science*, 84, 506
- El-Badry, K., Rix, H.-W., Cendes, Y., et al. 2023a, *MNRAS*, 521, 4323
- El-Badry, K., Rix, H.-W., & Heintz, T. M. 2021, *MNRAS*, 506, 2269
- El-Badry, K., Rix, H.-W., Latham, D. W., et al. 2024, *The Open Journal of Astrophysics*, 7, 58
- El-Badry, K., Rix, H.-W., Quataert, E., et al. 2023b, *MNRAS*, 518, 1057
- ESO. 2024, *The Extremely Large Telescope*, <https://www.eso.org/sci/facilities/eelt/>
- Event Horizon Telescope Collaboration, Akiyama, K., Alberdi, A., et al. 2022, *ApJ*, 930, L16
- Event Horizon Telescope Collaboration, Akiyama, K., Alberdi, A., et al. 2019, *ApJ*, 875, L5
- Feldmeier-Krause, A., Veršič, T., van de Ven, G., Gallego-Cano, E., & Neumayer, N. 2025, *A&A*, 699, A239
- Figer, D. F., Rich, R. M., Kim, S. S., Morris, M., & Serabyn, E. 2004, *ApJ*, 601, 319
- Frail, D. A., Polisenky, E., Hyman, S. D., et al. 2024, *ApJ*, 975, 34
- Freitag, M., Amaro-Seoane, P., & Kalogera, V. 2006, *ApJ*, 649, 91
- Fritz, T., Gillessen, S., Trippe, S., et al. 2010, *MNRAS*, 401, 1177
- Fritz, T. K., Chatzopoulos, S., Gerhard, O., et al. 2016, *ApJ*, 821, 44
- Fritz, T. K., Gillessen, S., Dodds-Eden, K., et al. 2011, *ApJ*, 737, 73
- Fujita, Y., Inoue, S., Nakamura, T., Manmoto, T., & Nakamura, K. E. 1998, *ApJ*, 495, L85
- Gaia Collaboration, Brown, A. G. A., Vallenari, A., et al. 2016, *A&A*, 595, A2
- Gaia Collaboration, Vallenari, A., Brown, A. G. A., et al. 2023, *A&A*, 674, A1
- Galishnikova, A., Philippov, A., Quataert, E., Chatterjee, K., & Liska, M. 2025, *ApJ*, 978, 148
- Gallego-Cano, E., Fritz, T., Schödel, R., et al. 2024, *A&A*, 689, A190
- Gautam, Do, T., Ghez, A. M., et al. 2019, *ApJ*, 871, 103
- Gautam, A. K., Do, T., Ghez, A. M., et al. 2024, *Astrophysical Journal*, 964, 164
- Geballe, T. R., Najarro, F., Rigaut, F., & Roy, J. R. 2006, *ApJ*, 652, 370
- Gelino, D. M., Balman, Ş., Kızıloğlu, Ü., et al. 2006, *ApJ*, 642, 438
- Generozov, A. & Madigan, A.-M. 2020, *ApJ*, 896, 137
- Generozov, A., Stone, N. C., Metzger, B. D., & Ostriker, J. P. 2018, *MNRAS*, 478, 4030
- Genzel, R., Eckart, A., Ott, T., & Eisenhauer, F. 1997, *MNRAS*, 291, 219
- Genzel, R., Eisenhauer, F., & Gillessen, S. 2010, *Reviews of Modern Physics*, 82, 3121
- Genzel, R., Schoedel, R., Alexander, T., et al. 2003, *The Astrophysical Journal*, 812
- Ghez, A. M., Becklin, E., Duchjné, G., et al. 2003, *Astronomische Nachrichten Supplement*, 324, 527
- Ghez, A. M., Klein, B. L., Morris, M., & Becklin, E. E. 1998, *Astrophysical Journal*, 509, 678
- Ghez, A. M., Salim, S., Weinberg, N. N., et al. 2008, *ApJ*, 689, 1044
- Giesers, B., Dreizler, S., Husser, T.-O., et al. 2018, *MNRAS*, 475, L15
- Gillessen, S., Eisenhauer, F., Trippe, S., et al. 2009, *ApJ*, 692, 1075
- Gillessen, S., Plewa, P. M., Eisenhauer, F., et al. 2017, *Astrophysical Journal*, 837, 30
- Gillessen, S., Plewa, P. M., Widmann, F., et al. 2019, *ApJ*, 871, 126
- Gilmozzi, R. & Spyromilio, J. 2007, *The Messenger*, 127, 11
- Gomel, R., Faigler, S., & Mazeh, T. 2021a, *MNRAS*, 504, 2115
- Gomel, R., Faigler, S., Mazeh, T., & Pawlak, M. 2021b, *MNRAS*, 504, 5907
- Gravity Collaboration, Abuter, R., Amorim, A., et al. 2024, *A&A*, 692, A242
- GRAVITY Collaboration, Abuter, R., Aimar, N., et al. 2022, *A&A*, 657, L12
- GRAVITY Collaboration, Abuter, R., Amorim, A., et al. 2018, *Astronomy & Astrophysics*, 615, L15
- Gravity Collaboration, Abuter, R., Amorim, A., et al. 2020, *Astronomy & Astrophysics*, 636, L5
- GRAVITY Collaboration, Abuter, R., Amorim, A., et al. 2019, *Astronomy & Astrophysics*, 625, L10
- Guo, M., Stone, J. M., Quataert, E., & Kim, C.-G. 2024, *ApJ*, 973, 141
- Habibi, M., Gillessen, S., Pfuhl, O., et al. 2019, *ApJ*, 872, L15
- Hailey, C. J., Mori, K., Bauer, F. E., et al. 2018, *Nature*, 556, 70
- Hills, J. G. 1988, *Nature*, 331, 687
- Hoang, B.-M., Naoz, S., Kocsis, B., Rasio, F. A., & Dosopoulou, F. 2018, *ApJ*, 856, 140
- Hoyle, F. & Lyttleton, R. A. 1939, *Proceedings of the Cambridge Philosophical Society*, 35, 405
- Jia, S., Xu, N., Lu, J. R., et al. 2023, *ApJ*, 949, 18
- Kennea, J. A., Burrows, D. N., Kouveliotou, C., et al. 2013, *ApJ*, 770, L24
- Krabbe, A., Genzel, R., Drapatz, S., & Rotaciuc, V. 1991, *ApJ*, 382, L19
- Kramer, M., Backer, D. C., Cordes, J. M., et al. 2004, *New A Rev.*, 48, 993
- Kramer, M. & Champion, D. J. 2013, *Classical and Quantum Gravity*, 30, 224009
- Kramer, M. & Stappers, B. 2015, in *Advancing Astrophysics with the Square Kilometre Array (AASKA14)*, 36
- Kremer, K., Spera, M., Becker, D., et al. 2020, *ApJ*, 903, 45
- Krivonos, R., Hailey, C., Mori, K., et al. 2021, in *Astronomical Society of the Pacific Conference Series*, Vol. 528, *New Horizons in Galactic Center Astronomy and Beyond*, ed. M. Tsuboi & T. Oka, 139
- Kroupa, P. 2001, *MNRAS*, 322, 231
- Kudo, Y., Negoro, H., Nakajima, M., et al. 2025, *The Astronomer’s Telegram*, 16975, 1
- Labaj, M., Ressler, S. M., Zajaček, M., et al. 2025, *A&A*, 702, A233
- Lalakos, A., Tchekhovskoy, A., Most, E. R., et al. 2025, *Phys. Rev. D*, 112, 123044
- Linial, I. & Sari, R. 2022, *ApJ*, 940, 101
- Liska, M., Tchekhovskoy, A., & Quataert, E. 2020, *MNRAS*, 494, 3656
- Lu, J. R., Do, T., Ghez, A. M., et al. 2013, *Astrophysical Journal*, 764, 155
- Lu, J. R., Ghez, A. M., Hornstein, S. D., et al. 2006, in *Journal of Physics Conference Series*, Vol. 54, *Journal of Physics Conference Series*, 279–287
- Madurga Favieres, C., Kissler-Patig, M., Xu, S., & Bonsor, A. 2024, *A&A*, 688, A168
- Mahy, L., Sana, H., Shenar, T., et al. 2022, *A&A*, 664, A159
- Mandel, S., Mori, K., Ciurlo, A., et al. 2025, arXiv e-prints, arXiv:2509.14465
- Maness, H., Martins, F., Trippe, S., et al. 2007, *ApJ*, 669, 1024
- Marconi, A., Abreu, M., Adibekyan, V., et al. 2024, in *Society of Photo-Optical Instrumentation Engineers (SPIE) Conference Series*, Vol. 13096, *Ground-based and Airborne Instrumentation for Astronomy X*, ed. J. J. Bryant, K. Motohara, & J. R. D. Vernet, 1309613
- Marklund, A., Church, R. P., & Trani, A. A. 2025, *A&A*, 702, A158
- Marra, L., Mikušinová, R., Vincentelli, F. M., et al. 2025, arXiv e-prints, arXiv:2506.17050

- Martins, F., Genzel, R., Hillier, D. J., et al. 2007, *A&A*, 468, 233
- Martins, F., Trippe, S., Paumard, T., et al. 2006, *ApJ*, 649, L103
- Masci, F. J., Laher, R. R., Rusholme, B., et al. 2019, *PASP*, 131, 018003
- Mashian, N. & Loeb, A. 2017, *MNRAS*, 470, 2611
- Massari, D., Fiorentino, G., Tolstoy, E., et al. 2016, in *Society of Photo-Optical Instrumentation Engineers (SPIE) Conference Series*, Vol. 9909, *Adaptive Optics Systems V*, ed. E. Marchetti, L. M. Close, & J.-P. Véran, 99091G
- Merritt, D., Alexander, T., Mikkola, S., & Will, C. M. 2010, *Phys. Rev. D*, 81, 062002
- Michail, J., von Fellenberg, S., Haggard, D., et al. 2025, *The Astronomer's Telegram*, 17174, 1
- Miralda-Escudé, J. & Gould, A. 2000, *ApJ*, 545, 847
- Moe, M. & Di Stefano, R. 2017, *ApJS*, 230, 15
- Morris, M. 1993, *ApJ*, 408, 496
- Morris, S. L. 1985, *ApJ*, 295, 143
- Morris, S. L. & Naftilan, S. A. 1993, *ApJ*, 419, 344
- Mroz, P. & Poleski, R. 2023, *arXiv e-prints*, arXiv:2310.07502
- Muno, M. P., Baganoff, F. K., Bautz, M. W., et al. 2003, *ApJ*, 589, 225
- Muno, M. P., Bauer, F. E., Baganoff, F. K., et al. 2009, *ApJS*, 181, 110
- Muno, M. P., Pfahl, E., Baganoff, F. K., et al. 2005, *ApJ*, 622, L113
- Mus, A., Marti-Vidal, I., Wielgus, M., & Stroud, G. 2022, *A&A*, 666, A39
- Newton, A., Rose, S. C., Kiroğlu, F., Hoang, B.-M., & Rasio, F. A. 2026, *arXiv e-prints*, arXiv:2602.04176
- Nitschai, M. S., Neumayer, N., & Feldmeier-Krause, A. 2020, *ApJ*, 896, 68
- Nogueras-Lara, F., Gallego-Calvente, A. T., Dong, H., et al. 2018, *A&A*, 610, A83
- Ott, T., Eckart, A., & Genzel, R. 1999, *ApJ*, 523, 248
- Pang, B., Pen, U.-L., Matzner, C. D., Green, S. R., & Liebendörfer, M. 2011, *MNRAS*, 415, 1228
- Paumard, T., Genzel, R., Martins, F., et al. 2006, *ApJ*, 643, 1011
- Peebles, P. J. E. 1972, *ApJ*, 178, 371
- Peißker, F., Zajaček, M., Labadie, L., et al. 2024, *Nature Communications*, 15, 10608
- Pen, U.-L., Matzner, C. D., & Wong, S. 2003, *ApJ*, 596, L207
- Pesce, D. W., Palumbo, D. C. M., Narayan, R., et al. 2021, *ApJ*, 923, 260
- Pfahl, E. & Loeb, A. 2004, *ApJ*, 615, 253
- Pfuhl, Alexander, T., Gillessen, S., et al. 2014, *ApJ*, 782, 101
- Pfuhl, O., Fritz, T. K., Zilka, M., et al. 2011, *ApJ*, 741, 108
- Plotkin, R. M., Gallo, E., Markoff, S., et al. 2015, *MNRAS*, 446, 4098
- Porquet, D., Grosso, N., Bélanger, G., et al. 2005, *A&A*, 443, 571
- Quataert, E. 2004, *ApJ*, 613, 322
- Rafelski, M., Ghez, A. M., Hornstein, S. D., Lu, J. R., & Morris, M. 2007, *ApJ*, 659, 1241
- Ressler, S. M., Quataert, E., & Stone, J. M. 2018, *MNRAS*, 478, 3544
- Ressler, S. M., Quataert, E., & Stone, J. M. 2020a, *MNRAS*, 492, 3272
- Ressler, S. M., Quataert, E., White, C. J., & Blaes, O. 2021, *MNRAS*, 504, 6076
- Ressler, S. M., White, C. J., & Quataert, E. 2023, *MNRAS*, 521, 4277
- Ressler, S. M., White, C. J., Quataert, E., & Stone, J. M. 2020b, *ApJ*, 896, L6
- Ricker, G. R., Winn, J. N., Vanderspek, R., et al. 2015, *Journal of Astronomical Telescopes, Instruments, and Systems*, 1, 014003
- Sahu, K. C., Anderson, J., Casertano, S., et al. 2022, *ApJ*, 933, 83
- Sana, H., de Koter, A., de Mink, S. E., et al. 2013, *A&A*, 550, A107
- Sana, H., Le Bouquin, J.-B., Lacour, S., et al. 2014, *ApJS*, 215, 15
- Schödel, R., Eckart, A., Alexander, T., et al. 2007, *A&A*, 469, 125
- Schödel, R., Gallego-Cano, E., Dong, H., et al. 2018, *Astronomy & Astrophysics*, 609, A27
- Schödel, R., Najarro, F., Muzic, K., & Eckart, A. 2010, *Astronomy and Astrophysics*, 511, A18
- Schödel, R., Nogueras-Lara, F., Gallego-Cano, E., et al. 2020, *Astronomy & Astrophysics*, 641, A102
- Schödel, R., Ott, T., Genzel, R., et al. 2002, *Nature*, 419, 694
- Shcherbakov, R. V. & Baganoff, F. K. 2010, *ApJ*, 716, 504
- Shenar, T., Sana, H., Mahy, L., et al. 2022a, *Nature Astronomy*, 6, 1085
- Shenar, T., Sana, H., Mahy, L., et al. 2022b, *A&A*, 665, A148
- Soberman, G. E., Phinney, E. S., & van den Heuvel, E. P. J. 1997, *A&A*, 327, 620
- Sturm, E., Davies, R., Alves, J., et al. 2024, in *Society of Photo-Optical Instrumentation Engineers (SPIE) Conference Series*, Vol. 13096, *Ground-based and Airborne Instrumentation for Astronomy X*, ed. J. J. Bryant, K. Motohara, & J. R. D. Vernet, 1309611
- Sumi, T., Udalski, A., Bennett, D. P., et al. 2016, *ApJ*, 825, 112
- Thatte, N., Tecza, M., Schnetler, H., et al. 2021, *The Messenger*, 182, 7
- The LIGO Scientific Collaboration, the Virgo Collaboration, the KAGRA Collaboration, et al. 2025, *arXiv e-prints*, arXiv:2508.18083
- Udalski, A., Szymański, M. K., & Szymański, G. 2015, *Acta Astron.*, 65, 1
- Volonteri, M. 2010, *A&A Rev.*, 18, 279
- von Fellenberg, S. D., Gillessen, S., Stadler, J., et al. 2022, *Astrophysical Journal*, 932, L6
- Wang, Q. D., Gottlieb, E. V., & Lang, C. C. 2002, *Nature*, 415, 148
- Wang, X. & Loeb, A. 2014, *MNRAS*, 441, 809
- Xu, W. 2023, *ApJ*, 954, 180
- Xu, W. & Stone, J. M. 2019, *MNRAS*, 488, 5162
- Xuan, Z., Naoz, S., Kocsis, B., & Michaely, E. 2024, *Phys. Rev. D*, 110, 023020
- Yelda, S., Ghez, A. M., Lu, J. R., et al. 2014, *ApJ*, 783, L31
- Zamaninasab, M., Clausen-Brown, E., Savolainen, T., & Tchekhovskoy, A. 2014, *Nature*, 510, 126
- Zhang, F. & Amaro Seoane, P. 2024, *ApJ*, 961, 232
- Zhao, J.-H., Blundell, R., Moran, J. M., et al. 2010, *ApJ*, 723, 1097
- Zhao, J.-H., Morris, M. R., & Goss, W. M. 2022, *ApJ*, 927, L6
- Zhao, J.-H., Morris, M. R., Goss, W. M., & An, T. 2009, *ApJ*, 699, 186
- Zhu, Z., Li, Z., & Morris, M. R. 2018, *ApJS*, 235, 26